

Applying Deep Learning to NASA MODIS Data to Create a Community Record of Marine Low Cloud Mesoscale Morphology

Tianle Yuan^{1,2}, Hua Song³, Robert Wood⁴, Johannes Mohrmann⁴, Kerry Meyer¹, Lazaros Oreopoulos¹, Steven Platnick¹

¹Earth Science Directorate, NASA Goddard Space Flight Center

²Joint Center for Earth Systems Technology, University of Maryland, Baltimore County

³Science Systems and Applications, Inc.

⁴Department of Atmospheric Sciences, University of Washington

Correspondence: tianle.yuan@nasa.gov

Abstract:

Marine low clouds display rich mesoscale morphological types, distinct spatial patterns of cloud fields. Being able to differentiate low cloud morphology offers a tool for the research community to go one step beyond bulk cloud statistics such as cloud fraction and advance the understanding of low clouds. Here we report the progress of [our](#) project that aims to create an observational record of low cloud mesoscale morphology at a near-global (60S-60N) scale. First, a training set is created by our team members manually labeling thousands of mesoscale (128x128) MODIS scenes into six different categories: stratus, closed cellular convection, disorganized convection, open cellular convection, clustered cumulus convection, and suppressed cumulus convection. Then we train a deep convolutional neural network model using this training set to classify individual MODIS scenes at 128x128 resolution, and test it on a test set. The trained model achieves a cross-type average precision of about 93%. We apply the trained model to 16 years of data over the Southeast Pacific. The resulting climatological distribution of low cloud morphology types show [both](#) expected and unexpected features and suggest [s](#) promising potential for low cloud studies as a data product.

1. Introduction

Marine low clouds are important for the mass, heat, and momentum transport in the planetary boundary layer (PBL) and between the PBL and free troposphere, the radiative energy balance of the climate, and the magnitude of feedback strength under climate change. Observations of marine low clouds are indispensable for advancing our understanding of these clouds for deriving new theories and insights and for model validation and constraining. Modern satellite observations have the advantage of providing global and long-term coverage. Current satellite products offer detailed pixel-level retrievals of cloud properties such as cloud optical depth, cloud droplet effective radius, and cloud phase. Most cloud classification schemes are based on either single pixel measurements or joint-histograms of two cloud properties.

Deleted: a

Deleted: NASA funded

43 However, marine low clouds are known to have various mesoscale morphology types since first
44 satellite observations of clouds became available (Agee and Dowell, 1974). These mesoscale
45 morphology types are created by the characteristic patterns into which clouds are organized
46 (Figure 1). Cloud mesoscale morphology types are not only phenological classifications of
47 satellite images, but also manifestation of complex mixture of underlying physical processes
48 (Atkinson and Zhang, 1996; Stevens et al., 2005; Wang and Feingold, 2009; Wood, 2012; Wood
49 and Hartmann, 2006). These physical processes are critical for fundamental understanding and
50 better modeling of marine low clouds because of their impact on mass, heat, and momentum
51 transport, on radiative energy balance, and their feedbacks to climate change. Wood and
52 Hartmann (2006) trained a two-layer neural network on probability distribution functions and
53 2-d power spectra of liquid water path to classify cloud morphology into four categories for
54 256x256 scenes. The method has been successfully used to analyze morphology types and
55 associated cloud properties (McCoy et al., 2017; Muhlbauer et al., 2014).

56
57 Here we introduce a NASA funded project to classify marine low cloud observations into six
58 different mesoscale morphology types based directly on full images without engineering
59 features. The goal is to produce a community data record that spans about two decades at
60 near-global scales that will enable the research community to go beyond bulk cloud statistics
61 and will advance our understanding of low-level mesoscale convective clouds through
62 exploiting the rich spatial information content of observations. Section 2 describes the data and
63 methodology; section 3 introduces preliminary results and section 4 gives discussions of future
64 plans and outlook of the data product; section 5 concludes.

65 66 **2. Data and methods**

67 68 a. Data source

69 The primary observational data for this study are from the MODerate resolution Imaging
70 Spectrometer (MODIS) onboard the Aqua satellite. We use reflectance from channels 1
71 ($0.65\mu\text{m}$), 3 ($0.47\mu\text{m}$), and 4 ($0.55\mu\text{m}$) and cloud optical depth, cloud droplet effective radius,
72 cloud mask, and cloud top height from the MODIS cloud product (Platnick et al., 2017) in
73 building up the training set. The spatial resolution of these parameters is 1km at nadir. The
74 cloud optical depth and effective radius retrievals are combined to produce cloud liquid water
75 path (Platnick et al., 2017). Reflectance from channel 4 is used for deep neural network model
76 training and inference, while the other MODIS observations and products are used for data
77 quality control, filtering, and contextual information, as explained below.

78
79 We first break MODIS images into 128×128 pixels scenes and filter out scenes that contain
80 significant fraction of high clouds (no more than 10%), defined as pixels with cloud top height
81 above 6km, or whose low cloud fraction is lower than 5%. We also exclude scenes whose
82 viewing zenith angle is greater than 45 degrees. Scenes with more than 10% land coverage are
83 also excluded. The resulting scenes are treated as dominated by marine low clouds.

84
85 For training purpose, we create auxiliary images that contain the broad context of the scene of
86 interest and distributions of the liquid water path and cloud top height for the scene (Figure 2).

Field Code Changed

Deleted: (Platnick et al., 2016)

Deleted: (Platnick et al., 2016)

Field Code Changed

89 The scene image together with the auxiliary images are presented to a panel of human experts
90 on the Zooniverse platform (www.zooniverse.org) for manual labeling. We intend to use the
91 same platform in the future to crowdsource the labeling task.

92
93 Spatiotemporally collocated Modern-Era Retrospective analysis for Research and Applications,
94 version 2 (MERRA-2) (Gelaro et al., 2017) data is used to provide meteorological variables for
95 each scene.

96 97 b. Morphology types

98 Marine low cloud mesoscale morphology patterns are extremely diverse. In order to keep the
99 task manageable, we settle on six representative types. They are stratus, closed cellular
100 convection, disorganized cellular convection, open cellular convection, clustered cumulus, and
101 suppressed cumulus (Figure 3). These types are by no means exhaustive given the diversity of
102 observable patterns. However, these six types are the most common and largely representative
103 of the data when we inspect a large collection of scenes. [In the current version, each low cloud
104 scene will be assigned one of these six types.](#) We also believe that these types have distinct
105 underlying physical processes. Stratus is mostly created by relatively uniform radiative cooling
106 or driven by synoptic weather systems such as fronts while closed cellular convection is driven
107 by radiative cooling and organized into distinctive honeycomb mesoscale patterns.
108 Disorganized cellular convection is characterized by a combination of elements of convection
109 and large portion of stratiform clouds that tend to have large droplet sizes and small cloud
110 optical depths, creating their characteristic appearance. Their cellular sizes are typically larger,
111 on the order of 100km, compared to closed cellular convection, on the order of 10km. Open
112 cellular convection is characterized by cells that are clear in the center and exhibit vigorous
113 shallow convection around it. These convective clouds are often precipitating based on satellite
114 and ship-based observations, which is a likely driving force that creates and maintains this
115 mesoscale morphology type (Wang and Feingold, 2009). Clustered cumulus convection is made
116 up of shallow, vigorous convective elements that aggregate together, accompanied by
117 scattered shallower and optically thinner cumulus clouds nearby. The suppressed cumulus type
118 is dominated by individual, scattered cumulus clouds that can sometimes have patterns like
119 lines and branches.

120 121 c. Method

122 To illustrate the difficulty of classifying morphology types using one-point statistics such as
123 histograms, we show the mean probability density functions (PDFs) of cloud optical depth and
124 droplet effective radius for each type in Figure 4. [We randomly select 1000 scenes for each
125 cloud type from 2006 data in the Southeast Pacific region.](#) The significant overlap between PDFs
126 of different types makes it quite hard to classify the scenes based on these PDFs. On the other
127 hand, deep convolutional neural network (DCNN) models have been shown to separate
128 complex patterns into different categories at a human level (LeCun et al., 2015). We apply a
129 transfer learning approach to our classification task in a supervised fashion although separate
130 efforts of unsupervised training also seem promising (Yuan, 2019).
131

Deleted: to keep the task manageable

133 Specifically, we use a pretrained model (Simonyan & Zisserman, 2015) as a feature extractor
134 and fine-tune it with our training set. The pretrained model is a 16-layer DCNN that is trained
135 on the large-scale ImageNet dataset (Deng et al., 2009). Its weights are fixed. We add three
136 additional layers to the pretrained model, called VGG-16 and train the resulting full model on
137 our training set, the fine-tuning step. The output of the full DCNN model is a six-element
138 vector whose elements sum up to 1 and are interpreted as the probability that the model
139 assigns to one of the corresponding types. We assign every scene to the type that has the
140 highest probability and therefore effectively we have a metric to measure how confident the
141 model is for each classification, which provides useful information for users who may apply
142 filters to the data.

143
144 To build the training set, our team together with several expert level volunteers first manually
145 labeled thousands of scenes using the Zooniverse online tool. We retain only those scenes that
146 are unambiguously belonging to a certain type to present the best possible training set, which
147 includes hundreds of samples for each type. We augment the training set by rotating each
148 scene by 90 and 180 degrees and also flipping the open cellular scenes to increase their sample
149 size. [The flipping operation is achieved by mirroring the original image across a horizontal axis.](#)

150 **3. Results**

151 Here we report results for the training, show the classification at work at a granule level and for
152 two typical low marine low cloud regimes: winter time mid-latitude region downwind of the
153 East Coast of US and Canada and sub-tropical Southeast Pacific region.

154 a. Training performance

155
156 The training asymptotically converges to a plateau in terms of accuracy pretty quickly, within
157 about 30 epochs (Figure 5). Around epoch 30, the validation accuracy reaches a maximum. The
158 training and validation accuracies are at around 98% and 93%. We save the model configuration
159 with the best validation accuracy. After training, the model is applied to a test set that it has
160 never seen before. The resulting confusion matrix is shown in Figure 6. [The confusion matrix](#)
161 [summarizes the classification prediction results. For each cloud type, or row, it shows the](#)
162 [percentage of correct predictions on the diagonal and percentages of incorrect predictions off](#)
163 [the diagonal.](#) The trained model achieves an average precision of about 93% across different
164 types. Open cellular and disorganized cellular convection, are the two morphology types with
165 the lowest accuracy mainly because they had the lowest number of training samples. With
166 further increase in training samples in the future, we are confident that corresponding
167 accuracies can be further improved. The biggest challenge for the model comes from separating
168 disorganized cellular, open cellular, and clustered cumulus types. It is also worth noting that
169 there is inherent uncertainty with the classification since even expert labelers sometimes
170 disagree on the same scenes.

171 b. An example granule

172
173 An example of a classified MODIS granule is shown in Figure 7. The classification results are
174 overlaid on the visible MODIS image as colored circles whose position represents the center of
175 corresponding 128x128 scene. This is a low cloud dominated granule with a complex mix of
176

177 different morphology types. The few missing scenes within the viewing zenith angle limits are
178 due to subvisible high clouds overlapping the visible low clouds, which is not rare even for these
179 low cloud dominated regions (Yuan and Oreopoulos, 2013), as well as a couple of scenes with
180 too little low clouds. One can visually confirm that the model performs quite well in picking up
181 morphology types and their transitions corroborating the results in Figure 5.

182
183 c. Test run over the wintertime Northwest Atlantic

184 During the winter, there can be many cold air outbreak events over the Northwest Atlantic
185 region. They create maritime low cloud systems with various mesoscale morphology types. We
186 apply our model to data in winter of 2011. We first filter the raw data to include only marine
187 low cloud scenes using the criteria discussed in section 2. The 128x128 pixel scenes are fed into
188 the trained DCNN model for classification. For each scene, we record its morphology type,
189 geolocation, time and save the 2-D MODIS cloud retrieval parameters such as cloud optical
190 depth, cloud droplet effective radius, and cloud top pressure. In this run, we do not oversample
191 the data and therefore scenes do not overlap with each other.

192
193 Figure 8 shows frequency of occurrence maps for each cloud type along with surface wind
194 vectors. Stratus clouds dominate in the Hudson Bay and Labrador Sea. They also frequently
195 appear over waters around Newfoundland and, to a lesser degree, along the east coast of US
196 and Canada. There is also a local maximum in the western part of the Gulf of Mexico. Closed
197 cellular type dominates the warm water of the Gulf Stream where cold continental air meets
198 the warm water, which induces large flux of moisture and heat from the ocean into the
199 boundary layer and gives rise to formation of low clouds. These low clouds mostly appear as the
200 closed cellular type according to MODIS. The disorganized type only appears in significant
201 quantity in the subtropics away from the coast. Open cellular clouds peak in the area south of
202 the Greenland and in the Labrador Sea and have a local maximum that is centered around
203 60°W and 35°N. Both are downwind of the closed cellular cloud peaks. The clustered and
204 suppressed cumulus clouds mostly occur in the subtropics and tropics.

205
206 d. Results over the Southeast Pacific region

207 We obtained all relevant Aqua MODIS level-1b and level-2 files for the Southeast Pacific region
208 (5°S-45°S, 70°W-125°W) between 2003 and 2018. The total volume of data is about 30 Tb. This
209 region is well known for the semi-permanent stratocumulus clouds.

210
211 Figure 9 shows the 16-year climatology of sea surface temperature (SST), estimated inversion
212 strength (EIS) (Wood and Bretherton, 2006), and frequency of occurrence maps for each
213 morphology type in the Southeast Pacific region. The frequency is normalized by the number of
214 total MODIS scenes, including both low cloud and non-low cloud ones.

215
216 Stratus clouds predominantly occur near coastal upwelling regions in the subtropics as well as
217 in the mid-latitude regions south of 40 degrees. Both features agree with our expectations.
218 Stratus can still occur in other parts of the domain, but with frequencies generally below 10%.
219 Their frequency significantly drops away from the local maxima in the mid-latitudes and along
220 the coast. The local maxima of stratus occurrence frequency coincide spatially with cold SST.

Deleted: the

222
223 The closed cellular type occurs most frequently about five hundred kilometers away from the
224 coastlines. The absolute maximum is located around 27°S and 75°W, which is also where EIS
225 peaks. Indeed, the frequency of closed cellular type roughly correlates with the EIS pattern. The
226 frequency of this type drops off from its peak location more gradually compared to that of the
227 stratus. Its frequency is nevertheless below 10% west of 90°W and the direction of the
228 frequency of occurrence gradient is almost east to west. The location of peak frequency for the
229 disorganized type is further away from the coast and occurs around 21°S and 89°W. The
230 frequency map of this type also has an overall correlation with the EIS west of 90°W.

231
232 The frequency map for the open cellular type is the most distinct. Its peak features a bullseye
233 pattern and occurs further downwind of the peak of the disorganized type, with a peak
234 frequency of only about 10%. This type also appears relatively frequently in the mid-latitudes
235 associated with mid-latitude cyclones. Its spatial pattern has no direct correlation with either
236 EIS or SST patterns, possibly implying internal mechanisms that are responsible for their
237 appearances. Both the closed and open cellular locations agree qualitatively with the findings
238 from Wood and Hartmann (2006), although the addition of other cloud types resulted in lower
239 frequencies of these types in our dataset. It is also worth mentioning that the disorganized
240 cellular type has a different geographic occurrence when compared to Wood and Hartmann
241 (2006). This is because under that classification scheme, 'disorganized' includes the bulk of
242 scenes which we classify as suppressed and clustered; the more narrowly-defined disorganized
243 cellular type in our classification is geographically more closely associated with the other
244 cellular cloud types. The clustered cumulus type occurrence appears to have a general
245 anticorrelation with the EIS map. The suppressed cumulus type occurs most frequently in the
246 tropics where the SST is the warmest.

247 248 **4. Discussions and future work**

249 a. Notable new insights

250 Open cellular clouds are less prevalent than previously thought (Atkinson and Zhang, 1996;
251 McCoy et al., 2017; Muhlbauer et al., 2014), especially in subtropical regions. We attribute this
252 to the combination of advanced quantitative observation techniques developed here and the
253 delineation of clustered cumulus and open cellular types. The early studies did not have
254 comprehensive observations to rely on. The more recent results may have included the two
255 types together into the open cellular type, which overestimated the occurrence frequency of
256 the open cellular type in the subtropics. However, given the relatively minor presence of
257 clustered cumulus type in the midlatitudes, the open cellular type may indeed be quite
258 prevalent there, which agrees with previous studies.

259
260 There is a strong spatial correlation between both EIS and SST and the frequency of stratus in
261 two regions analyzed, especially north of 35°N, suggesting a strong control of atmospheric
262 stability and cold SST on this cloud type in higher latitude regions. Their control on other cloud
263 types may not be as tight given the loose spatial correspondence between both EIS and SST and
264 frequency of other cloud types, implying either other large-scale variables are in control or
265 internal cloud processes are more important. We will leave such explorations for future studies.

266

267 b. Expanding the scale of test runs and further analysis

268 We plan to expand the test run to near-global scales for about two years. These runs will
269 include time periods that overlap those of several field campaigns that have rich in-situ and
270 ground and airborne remote sensing data. Together with these datasets, the satellite product
271 will help to advance the understanding of low cloud mesoscale morphology. The global scale
272 will also allow us to examine the general distributions of morphology types and intercompare
273 the characteristics of low cloud morphology in different ocean basins. Further data analysis of
274 the current test run and future runs will target questions related to the variability of low cloud
275 morphology and its driving forces. We plan to release part or all of the test run results to beta
276 testers for feedback and test use from the community.

277

278 c. Collocating with other satellite sensors and meteorology

279 We plan to collocate each classified low cloud scene with data from sensors like CloudSat cloud
280 profiling radar, CALIOP lidar, the Advanced Microwave Scanning Radiometer for EOS (AMSR-E
281 and AMSR-2), and Atmospheric InfraRed Sounder (AIRS) as well as the MERRA-2 reanalysis
282 products. Such collocated set of variables will be useful to the research community for studying
283 the behavior of low cloud morphology under different environmental conditions

284

285 d. Further improvement of the model

286 The current model works pretty well overall, particularly for closed cellular, suppressed
287 cumulus and clustered cumulus types. However, there is room to improve for other types. We
288 target two fronts for improvement: improving the model itself and increasing the quality and
289 quantity of training data. For the former goal, we plan to test different pre-trained models and
290 what features to keep and how to best set up the classifier on top of these extracted feature
291 vectors. For the latter goal, we have developed analysis tools to help us understand the
292 agreement among human experts in the training set. This helps us to target types that need the
293 improvement. We will use the Zooniverse tool to achieve this. Further increase in training data
294 also allows us to better characterize the uncertainty in expert labeling of each category. We are
295 looking for expert level volunteers to join us to increase the training sample size.

296

297 e. Increasing the number of types

298 Some of the mesoscale types can be further divided into subtypes. For example, the frequency
299 of suppressed cumulus type is quite high in the low latitudes and based on the manual labeling
300 they could be further divided into multiple subtypes. We will explore the feasibility of this by
301 assessing resource constraints and the feedback from the community.

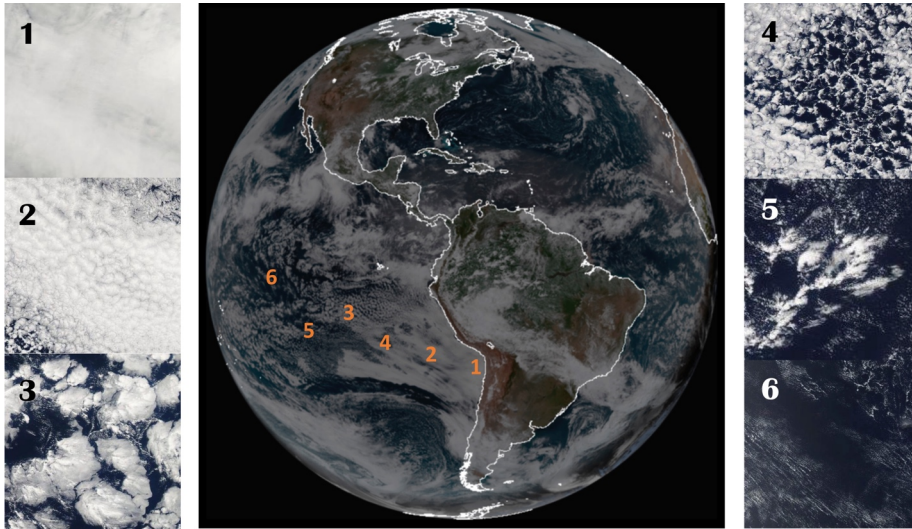
302

303

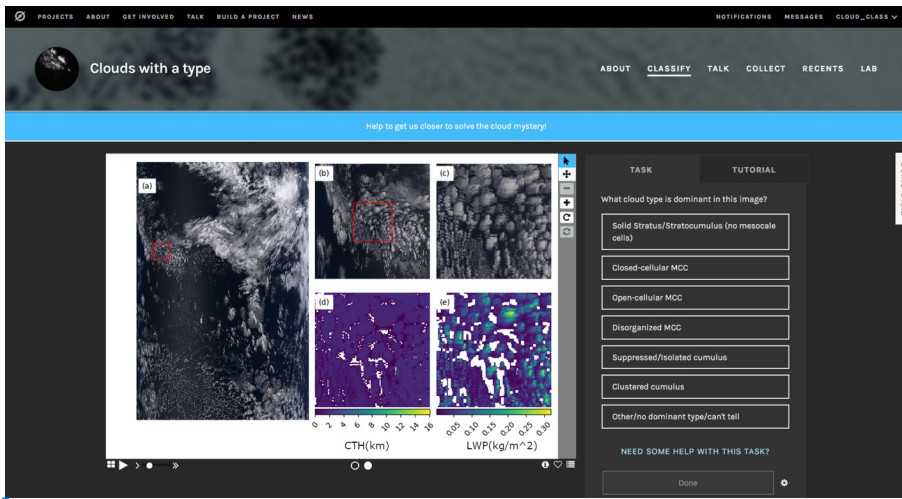
304 **5. Conclusions**

305 We have developed a working deep neural network model to automatically classify cloudy
306 scenes into six mesoscale morphology types. Initial test run results showed promising results
307 for the Southeast Pacific and Northwest Atlantic. Using the tool, we plan to extend the dataset
308 and create a community mesoscale morphology type product for low marine clouds observed

309 by MODIS. We will further develop the product and actively look forward to community
310 involvement such as beta testing, volunteering, and user feedback.
311
312

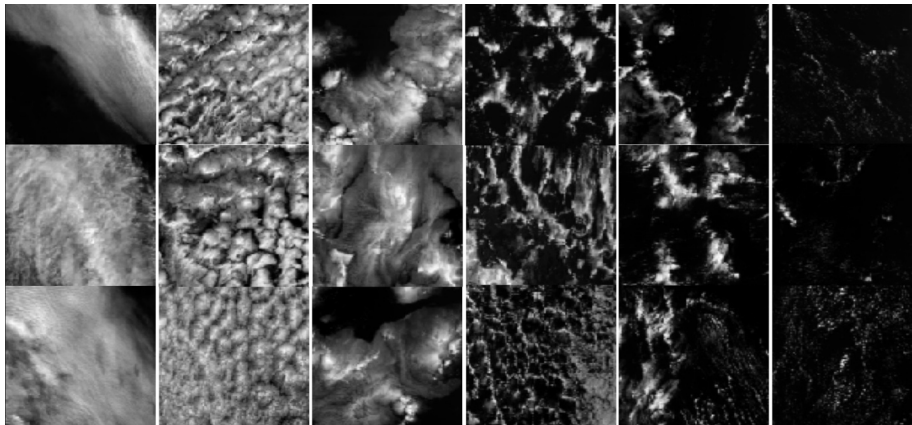


313
314 Figure 1: A full disk image of GOES-16 on Aug 6, 2018 and six scenes of MODIS images at smaller
315 scales representing different morphology types at corresponding locations in the GOES image.
316 Except scene 1, all scenes are from the same day. Scene 1 is from a different day because there
317 was no representative stratus scenes on this day in the Southeast Pacific region.
318
319

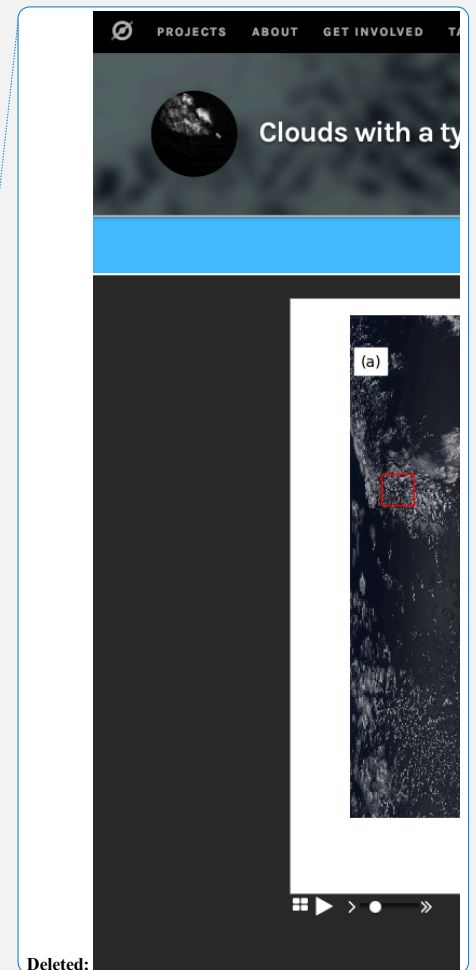


320
 321 Figure 2: the Zooniverse interface for manual labelling. The center image is made up of five
 322 panels. Panel a shows the full granule (usually 2030x1350 pixels) true color image for large
 323 context. Panel b shows a portion of the granule immediately surrounding the scene to be
 324 labelled, outlined by the red square. Panel c shows the visible scene image while panels d and e
 325 show the cloud top height and LWP fields in the scene to be labelled. The panels to the right of
 326 the center image show labelling choices. The tutorial document is available by clicking on the
 327 'FIELD GUIDE' tab on the right side. Additional options for scenes with heavily mixed types,
 328 scenes with sea ice, or scenes with other issues are found in the 'other' menu. The image is a
 329 screenshot of our Zooniverse project.

330
 331

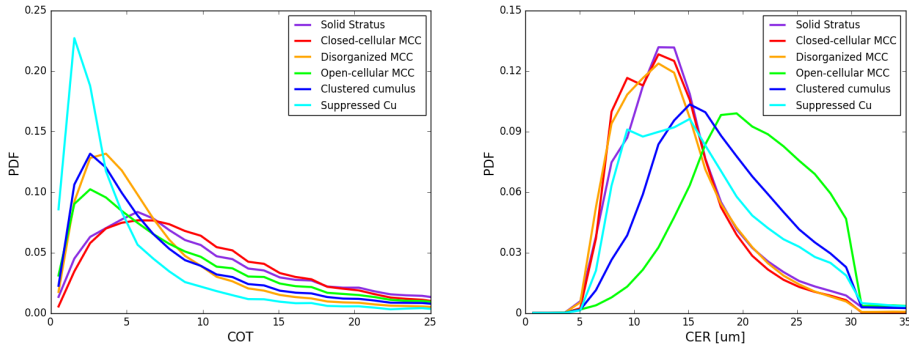


332
 333



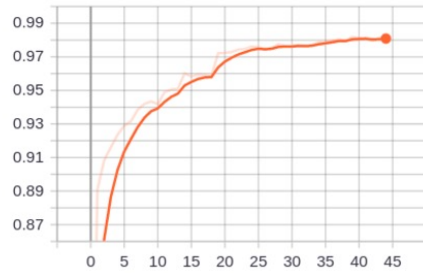
Deleted:

335 Figure 3: Example scenes of MODIS single channel images for the six different types. From left
 336 to right: stratus, closed cellular, disorganized cellular, open cellular, clustered cumulus, and
 337 suppressed cumulus types. Images taken by the NASA MODIS.
 338

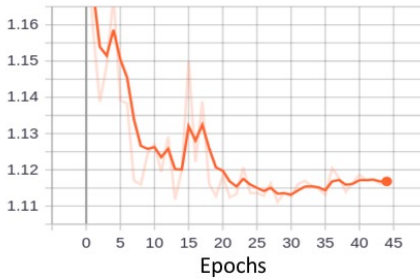
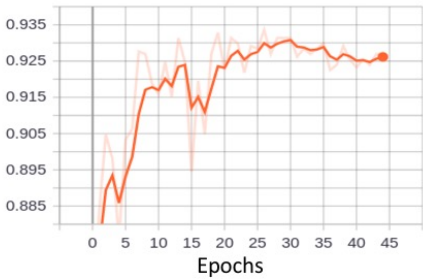
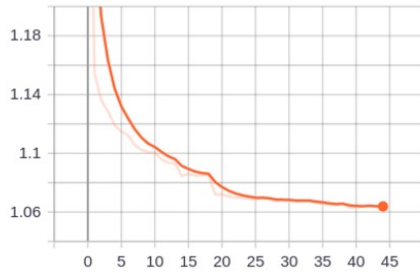


339
 340
 341 Figure 4: PDFs of cloud optical depth and cloud effective radius for six morphology types.
 342 Significant overlaps are observed for PDFs of both variables among different morphology types.
 343
 344

accuracy

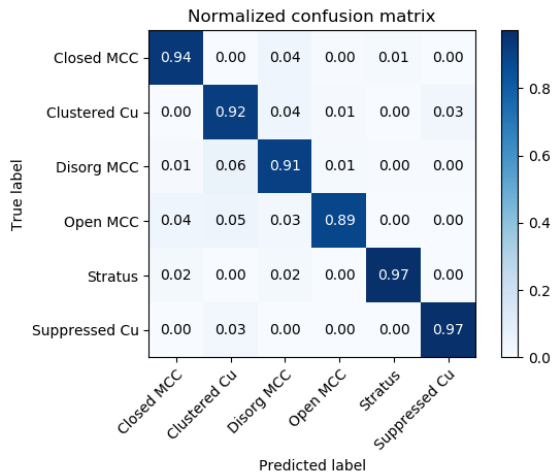


loss

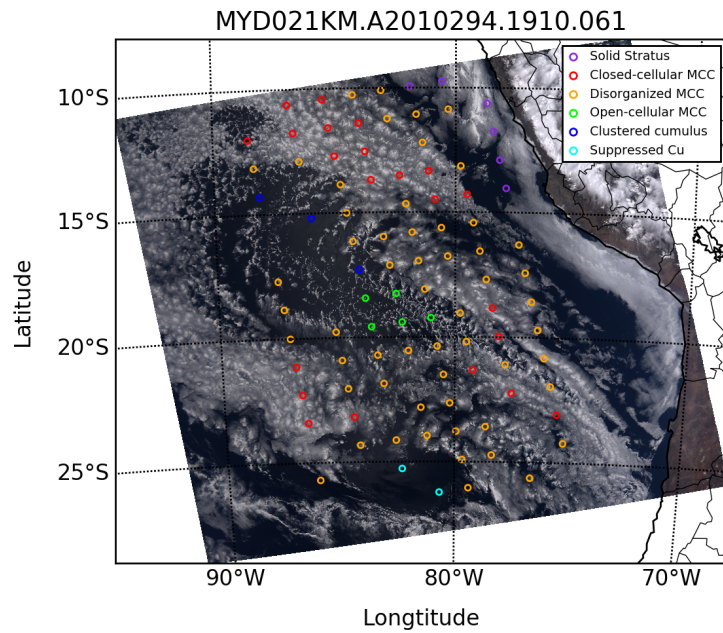


345

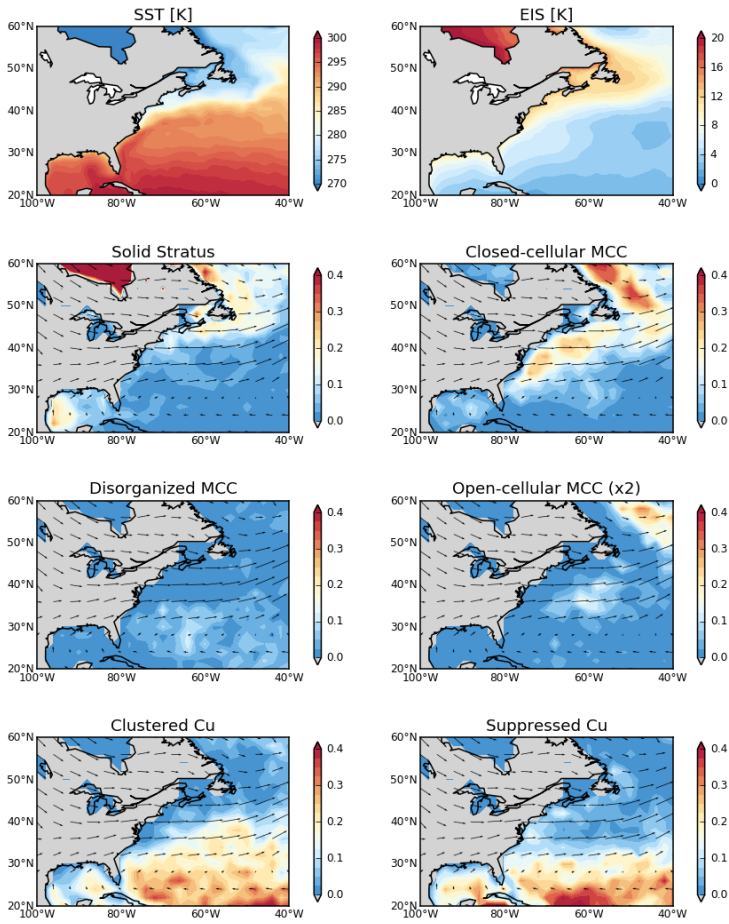
346 Figure 5: Training (upper two panels) and validation (lower ones) accuracy and loss trajectories.
 347 By around epoch 30, the validation accuracy peaks while validation loss bottoms out and the
 348 training loss and accuracy asymptotically reach their minimum and maximum, respectively,
 349 which indicates further training may be overfitting the model.
 350



351 Figure 6: Confusion matrix of the model predictions on test data.
 352

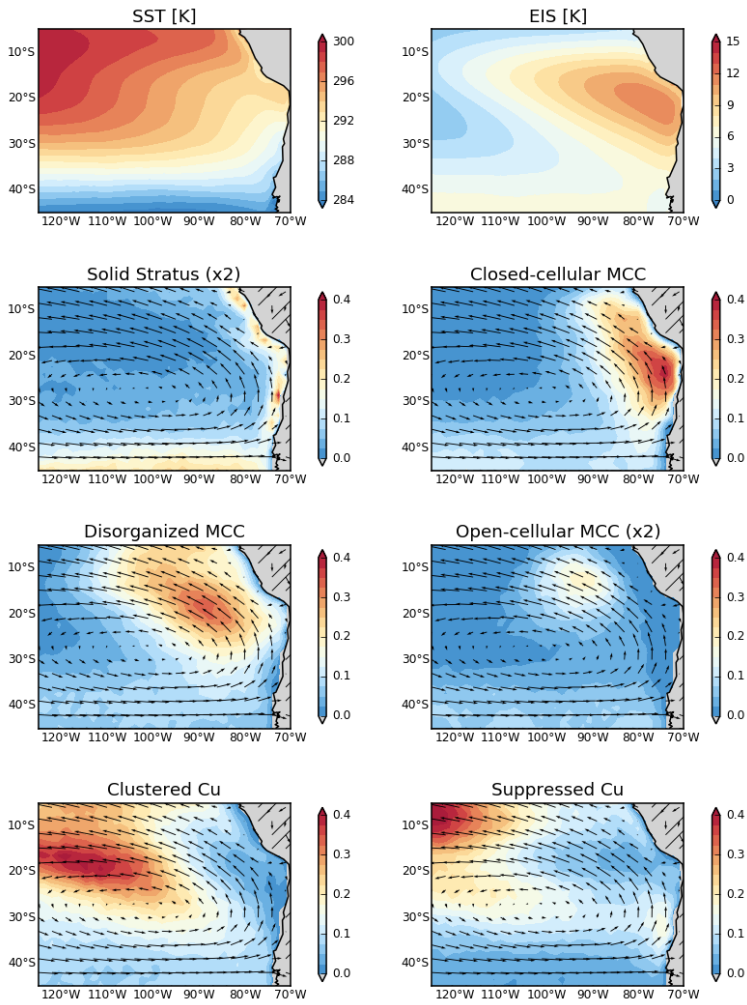


353
 354 Figure 7: An example granule illustrating the results of the classification algorithm. This is quite
 355 a complex granule with different morphology types mixed together. The left and right margins
 356 are not classified because current algorithm filters out scenes whose sensor viewing zenith
 357 angles are greater than 45 degrees. The image is taken by NASA MODIS.
 358



359
 360
 361
 362
 363
 364
 365
 366

Figure 8: Frequency distributions of six morphology types obtained from the classification algorithm in the Northwest Atlantic region off the east coasts of US and Canada in the winter of 2011. The top two panels show the SST and EIS distributions using MERRA-2. Seasonal mean wind vectors at 850hPa are plotted to illustrate the flow. We double the values for frequency of the open-cellular type to make them numerically comparable with other types.



367
 368 Figure 9: Frequency distributions of various morphology types obtained from the classification
 369 algorithm in the subtropical eastern Pacific off the coast of South America for the period 2003-
 370 2018. The top two panels show the SST and EIS climatology from MERRA-2 for the same period.
 371 Note the doubling of scale on the stratus and open-cellular types.

372
 373 **6. Author Contribution**

374 T. Y. implemented the method to train the network model. H. S., J. M., and T.Y. prepared the
375 training data. All co-authors contributed to compiling the training dataset. T. Y. wrote the
376 manuscript with contributions from [all](#) co-authors.
377

Deleted:

Deleted: other

378 7. Reference

379 [Agee, E. M., & Dowell, K. E. \(1974\). Observational Studies of Mesoscale Cellular Convection.](#)

Formatted: Font: (Default) Calibri

380 [Journal of Applied Meteorology, 13\(1\), 46–53. https://doi.org/10.1175/1520-](#)

Formatted: Bibliography, Automatically adjust right indent when grid is defined, Widow/Orphan control, Adjust space between Latin and Asian text, Adjust space between Asian text and numbers

381 [0450\(1974\)013<0046:OSOMCC>2.0.CO;2](#)

382 [Atkinson, B. W., & Zhang, W. J. \(1996\). Mesoscale shallow convection in the atmosphere.](#)

383 [Reviews Of Geophysics, 34\(4\), 403–431. https://doi.org/10.1029/96RG02623](#)

384 [Deng, J., Dong, W., Socher, R., Li, L.-J., Kai Li, & Li Fei-Fei. \(2009\). ImageNet: A large-scale](#)

385 [hierarchical image database. In *2009 IEEE Conference on Computer Vision and Pattern*](#)

386 [Recognition \(pp. 248–255\). https://doi.org/10.1109/CVPR.2009.5206848](#)

387 [Gelaro, R., McCarty, W., Suárez, M. J., Todling, R., Molod, A., Takacs, L., et al. \(2017\). The](#)

388 [Modern-Era Retrospective Analysis for Research and Applications, Version 2 \(MERRA-2\).](#)

389 [Journal of Climate, 30\(14\), 5419–5454. https://doi.org/10.1175/JCLI-D-16-0758.1](#)

390 [LeCun, Y., Bengio, Y., & Hinton, G. \(2015\). Deep learning. *Nature*, 521\(7553\), 436–444.](#)

391 [https://doi.org/10.1038/nature14539](#)

392 [McCoy, I. L., Wood, R., & Fletcher, J. K. \(2017\). Identifying Meteorological Controls on Open and](#)

393 [Closed Mesoscale Cellular Convection Associated with Marine Cold Air Outbreaks.](#)

394 [Journal of Geophysical Research: Atmospheres, 122\(21\), 11,678-11,702.](#)

395 [https://doi.org/10.1002/2017JD027031](#)

398 [Muhlbauer, A., McCoy, I. L., & Wood, R. \(2014\). Climatology of stratocumulus cloud](#)
399 [morphologies: microphysical properties and radiative effects. *Atmospheric Chemistry*](#)
400 [And Physics, 14\(13\), 6695–6716. <https://doi.org/10.5194/acp-14-6695-2014>](#)

401 [Platnick, S., Meyer, K. G., King, M. D., Wind, G., Amarasinghe, N., Marchant, B., et al. \(2017\). The](#)
402 [MODIS Cloud Optical and Microphysical Products: Collection 6 Updates and Examples](#)
403 [From Terra and Aqua. *IEEE Transactions on Geoscience and Remote Sensing*, 55\(1\), 502–](#)
404 [525. <https://doi.org/10.1109/TGRS.2016.2610522>](#)

405 [Simonyan, K., & Zisserman, A. \(2015\). Very Deep Convolutional Networks for Large-Scale Image](#)
406 [Recognition. *ArXiv:1409.1556 \[Cs\]*. Retrieved from <http://arxiv.org/abs/1409.1556>](#)

407 [Stevens, B., Vali, G., Comstock, K., Wood, R., van Zanten, M. C., Austin, P. H., et al. \(2005\).](#)
408 [Pockets of open cells and drizzle in marine stratocumulus. *Bulletin Of The American*](#)
409 [Meteorological Society, 86\(1\), 51–—. <https://doi.org/10.1175/BAMS-86-1-51>](#)

410 [Wang, H., & Feingold, G. \(2009\). Modeling mesoscale cellular structures and drizzle in marine](#)
411 [stratocumulus. Part I: Impact of drizzle on the formation and evolution of open cells.](#)
412 [Journal Of The Atmospheric Sciences, 66\(11\), 3237–3256.](#)
413 [https://doi.org/10.1175/2009JAS3022.1](#)

414 [Wood, R., & Bretherton, C. S. \(2006\). On the relationship between stratiform low cloud cover](#)
415 [and lower-tropospheric stability. *Journal Of Climate*. Retrieved from](#)
416 [http://journals.ametsoc.org/doi/pdf/10.1175/JCLI3988.1](#)

417 [Wood, Robert. \(2012\). Stratocumulus Clouds. *Monthly Weather Review*, 140\(8\), 2373–2423.](#)
418 [https://doi.org/10.1175/MWR-D-11-00121.1](#)

419 [Wood, Robert, & Hartmann, D. L. \(2006\). Spatial variability of liquid water path in marine low](#)
420 [cloud: The importance of mesoscale cellular convection. *Journal Of Climate*, 19\(9\),](#)
421 [1748–1764.](#)

422 [Yuan, T. \(2019\). Understanding Low Cloud Mesoscale Morphology with an Information](#)
423 [Maximizing Generative Adversarial Network. <https://doi.org/10.31223/osf.io/gvebt>](#)

424 [Yuan, T., & Oreopoulos, L. \(2013\). On the global character of overlap between low and high](#)
425 [clouds. *Geophysical Research Letters*, 40\(19\), 5320–5326.](#)
426 <https://doi.org/10.1002/grl.50871>

427
428
429
430
431
432
433
434
435
436
437
438
439
440
441
442
443
444
445
446
447
448
449
450
451
452
453

Deleted: Agee, E. M., & Dowell, K. E. (1974). Observational Studies of Mesoscale Cellular Convection. *Journal of Applied Meteorology*, 13(1), 46–53. [https://doi.org/10.1175/1520-0450\(1974\)013<0046:OSOMCC>2.0.CO;2](https://doi.org/10.1175/1520-0450(1974)013<0046:OSOMCC>2.0.CO;2)

Atkinson, B. W., & Zhang, W. J. (1996). Mesoscale shallow convection in the atmosphere. *Reviews Of Geophysics*, 34(4), 403–431. <https://doi.org/10.1029/96RG02623>

Deng, J., Dong, W., Socher, R., Li, L.-J., Kai Li, & Li Fei-Fei. (2009). ImageNet: A large-scale hierarchical image database. In *2009 IEEE Conference on Computer Vision and Pattern Recognition* (pp. 248–255). <https://doi.org/10.1109/CVPR.2009.5206848>

Gelaro, R., McCarty, W., Suárez, M. J., Todling, R., Molod, A., Takacs, L., et al. (2017). The Modern-Era Retrospective Analysis for Research and Applications, Version 2 (MERRA-2). *Journal of Climate*, 30(14), 5419–5454. <https://doi.org/10.1175/JCLI-D-16-0758.1>

LeCun, Y., Bengio, Y., & Hinton, G. (2015). Deep learning. *Nature*, 521(7553), 436–444. <https://doi.org/10.1038/nature14539>

McCoy, I. L., Wood, R., & Fletcher, J. K. (2017). Identifying Meteorological Controls on Open and Closed Mesoscale Cellular Convection Associated with Marine Cold Air Outbreaks. *Journal of Geophysical Research: Atmospheres*, 122(21), 11,678–11,702. <https://doi.org/10.1002/2017JD027031>

Muhlbauer, A., McCoy, I. L., & Wood, R. (2014). Climatology of stratocumulus cloud morphologies: microphysical properties and radiative effects. *Atmospheric Chemistry And Physics*, 14(13), 6695–6716. <https://doi.org/10.5194/acp-14-6695-2014>

Platnick, S., Meyer, K. G., King, M. D., & Wind, G. (2016). The MODIS Cloud Optical and Microphysical Products: Collection 6 Updates and Examples From Terra and Aqua. *Journal of Geoscience and Technology*. Retrieved from <http://ieeexplore.ieee.org/abstract/document/7707459/>

Simonyan, K., & Zisserman, A. (2015). Very Deep Convolutional Networks for Large-Scale Image Recognition. *ArXiv:1409.1556 [Cs]*. Retrieved from <http://arxiv.org/abs/1409.1556>

Stevens, B., Vali, G., Comstock, K., Wood, R., van Zanten, M. C., Austin, P. H., et al. (2005). Pockets of open cells and drizzle in marine stratocumulus. *Bulletin Of The American Meteorological Society*, 86(1), 51–—. <https://doi.org/10.1175/BAMS-86-1-51>

Wang, H., & Feingold, G. (2009). Modeling mesoscale cellular structures and drizzle in marine stratocumulus. Part I: Impact of drizzle on the formation and evolution of open cells. *Journal Of The Atmospheric Sciences*, 66(11), 3237–3256. <https://doi.org/10.1175/2009JAS3022.1>

Wood, R., & Bretherton, C. S. (2006). On the relationship between stratiform low cloud cover and lower-tropospheric stability. *Journal Of Climate*. Retrieved from <http://journals.ametsoc.org/doi/pdf/10.1175/JCLI3988.1>

Wood, Robert. (2012). Stratocumulus Clouds. *Monthly Weather Review*, 140(8), 2373–2423. <https://doi.org/10.1175/MWR-D-11-00121.1> ... [1]

582 **Point-by-point response to reviewers:**

583
584
585 **We would like to thank the reviewers for their suggestions, edits and questions which**
586 **contributed to a hopefully improved revised manuscript. In the following, please find our**
587 **point by point response to the reviewer’s comments.**

588
589 *Anonymous Referee #1*

590 *Received and published: 30 April 2020*

591
592 *Yuan et al. present a method to identify marine low-level cloud regimes. Using MODIS*
593 *reflectances, and creating a training dataset by human visual inspection, they apply a Deep*
594 *convolutional neural network to objectively assign each scene to one of six pre-defined types.*
595 *The method is well described and carefully evaluated. The authors aim to make their product*
596 *publicly available which is potentially of great usefulness to studies of clouds. The paper is very*
597 *well written and of interest to the readership of Atmos. Meas. Tech. I only have a few minor*
598 *remarks which the authors should consider in a revision.*

599
600 *127 “shows”*

601 **Changed.**

602
603 *128 “suggests”*

604 **Changed.**

605
606 *139 “histograms”; however aren’t pixel-level retrievals and joint histograms redundant? the*
607 *latter is just a way to statistically retain the pixel-level information at level 3 aggregation.*
608 **Correct. It depends on how the pixel-level retrievals are used. But ultimately, they both use**
609 **the pixel level retrievals. Some methods use a one-dimensional PDF and others may use**
610 **joint-histograms.**

611
612 *141 only since then? Or not rather since ever / since the first cloud observations (such as*
613 *Howard.*

614 **The reference we used is the best example we are aware of. Could the reviewer provide us**
615 **with a complete reference?**

616
617 *162 “a plan” or “plans”*

618 **Changed.**

619
620
621 *170 The Platnick reference should be updated (actual author list is longer, and it appeared 2017*
622 *(vol 55)).*

623 **Changed.**

624
625 *171 Please specify the horizontal resolution for reflectances and retrieval products.*

626 **Added.**

628
629
630
631
632
633
634
635
636
637
638
639
640
641
642
643
644
645
646
647
648
649
650
651
652
653
654
655
656
657
658
659
660
661
662
663
664
665
666
667
668
669
670
671
672
673

177 Provide the unit here. I assume it is 128 x 128 pixels of 1x1 km² size each?

Changed. Since the pixel size changes slightly with view angle we now simply quote scene size in terms of pixels rather than physical area.

184 It is a nice idea to include this a bit technical detail. This illustrated well what is actually done.

187 And this is a good idea!

Thanks!

194 Omit “keep the task manageable” once.

Changed.

1119 Are the PDFs exactly the retrievals from the scenes provided in Fig. 3? It would be good if it was such, and should be clarified in the text.

The PDFs are mean distributions of samples belonging to a particular type. We randomly selected 1000 scenes for each cloud type.

1141 I don’t understand what “flipping” means if not rotating by 180°. The authors should clarify this.

Now clarified.

1154 It would be useful to explain in one sentence to the non-specialized readership what the confusion matrix is.

Now explained.

1161 It would be interesting to know how often this occurs for the different cloud types. E.g. a fraction of disagreement for each type?

With the added explanation about the confusion matrix, readers should be able to read how often misclassifications occur for each type and how they distribute across different types.

1165 This mostly looks quite reasonable. However, some results seem rather strange to the naked eye. E.g. where the solid stratus diagnosed at 14°S/78°W I don’t see any cloud, let alone a stratus.

The dot represents the center location of a scene. The right half of this scene is indeed occupied by stratus clouds. A scene does not have to be mostly cloudy to be classified as stratus. The algorithm examines the textual information of the clouds.

1186 drop “the”

Changed.

674 *1338 “indicates”. And what is the difference between the light pink and red lines?*
675 **Changed. The solid lines are running means of the light pink lines.**

676
677
678 *1365 Help from which other authors?*
679 **Clarified.**

680
681 **We would like to thank the reviewers for their suggestions, edits and questions which**
682 **contributed to a hopefully improved revised manuscript. In the following, please find our**
683 **point by point response to the reviewer’ comments.**

684
685 *Anonymous Referee #2*

686
687 *Received and published: 4 May 2020*

688
689 *The authors report an interesting work of applying a deep learning model to 16 years of satellite*
690 *data to create an observational classification of marine low cloud mesoscale morphology. The*
691 *deep learning technique is quite novel in this area of remote sensing measurement and analysis.*
692 *The science topic is also of interest to the atmospheric and climate science community. The*
693 *paper is well written. I only have a few minor comments and questions for the authors to*
694 *consider for improving the presentation quality of the paper.*

695
696 *Specific comments:*

697 *Line 18: Considering that AMT is an international journal, the authors might want to clarify on*
698 *“NASA funded project” or remove it (which I don’t think is critical to mention here)*
699 **Changed.**

700
701
702 *Line 21, Line 52, Line 77: Are these (128x128 or 256x256) the number of pixels? Is the pixel size*
703 *250 m? Please clarify in the main text. I wonder how the size of each scene has been determined.*
704 *I imagine that a too big or too small size might cause some ambiguity in the classification of*
705 *mesoscale cloud morphology. For example, some of the disorganized MCC scenes in Figure 7*
706 *look like evolving open-cell or closed-cell MCC. Have any sensitivity tests been performed to*
707 *decide on the scene size for the training data?*

708 **Great point. We indeed spent months thinking about this question before deciding on**
709 **128x128 pixels. The pixel size is close to 1km. The main consideration is that if the size gets**
710 **too large, e.g. 256x256, the chance of mixed types in a scene increases. On the other hand, if**
711 **the size is too small, the lack of context renders classification by even humans hard because**
712 **it can become quite ambiguous.**

713
714 **The example you raised for Figure 7 is important in showing that the scale really matters.**
715 **The difference is more apparent at the native 128x128 scale. Looking at the scene when**
716 **zooming out, some of the disorganized MCCs indeed can be confused with open-cell MCC.**

717
718 *Line 97-98: Except for the scenes got filtered out, does each scene have to belong to one of the*
719 *six types when being analyzed for the frequency distribution? Please clarify.*

720 **Yes. We added a sentence for this point.**
721
722 *Line 105: Is the droplet size information used for disorganized MCC in the classification*
723 *algorithm? This could be useful to remove ambiguity mentioned above.*
724 **We did not include the droplet size information. It would indeed provide extra information**
725 **in many circumstances. However, including it would make the algorithm less general. We**
726 **opt to not include it in this trade-off.**
727
728 *Line 141: how does rotating or flipping scenes help to increase the open-cell MCC sample size?*
729 *That makes me wonder how the orientation of each scene affects the pattern recognition of the*
730 *deep learning model here.*
731 **Rotating and flipping are standard operations to enhance the sample size as well as the**
732 **robustness of the algorithm. A robust algorithm should be agnostic to orientation and**
733 **vantage point. We increased the sample size of open-cell scenes to reduce the imbalance**
734 **between cloud types.**
735
736 *Line 160-162: Was each scene in the training dataset labeled by at least two people? How if*
737 *there is a disagreement?*
738 **Not every scene was repeatedly labelled by two experts, but there are hundreds of scenes**
739 **that are labeled by at least two experts. When there is disagreement, an accompanying**
740 **discussion can be found online. In these situations, we also examine the scenes closely to**
741 **determine the true label.**
742
743 *Line 226-227: Please clarify on the “internal mechanisms”. Are you referring to the self-*
744 *organizing mechanisms (e.g., Feingold et al., 2010)? Feingold G, Koren I, Wang H, Xue H,*
745 *Brewer WA. (2010): Precipitation-generated oscillations in open-cellular cloud fields. Nature*
746 *466:doi:10.1038/nature09314.*
747 **Here we are making broad separations between two camps, one advocating for large-scale**
748 **forcing and the other for an internal mechanism. But yes, this paper would definitely count**
749 **as supporting the internal mechanism hypothesis.**
750
751 *Line 330: More details are needed for the PDFs in Figure 4. How many scenes? What time*
752 *periods and regions?*
753 **Good point. We added relevant information in the revision. We randomly selected 1000**
754 **scenes for each cloud type from 2006 data in the southeast Pacific region.**
755
756 *Line 78: No more than 10% of the scenes got filtered out? Please clarify.*
757 **Changed to clarify. We remove scenes with more than 10% land cover.**
758
759 *Line 117: classify -> classifying Line 146: remove the first “low”*
760 **Changed.**
761
762
763 *Line 311: units of LWP in Figure 2 are wrong.*
764 **Nice catch! Changed.**
765

766
767

1